

# Cellular Uptake and Intracellular Cargo Release From Dextran Based Nanogel Drug Carriers

**M. Carme Coll Ferrer**<sup>1</sup>

Department of Anesthesiology and Critical Care  
and Department of Materials  
Science and Engineering,  
University of Pennsylvania,  
Philadelphia, PA 19104

**Peter Sobolewski**<sup>1</sup>

Department of Anesthesiology and Critical Care,  
University of Pennsylvania,  
Philadelphia, PA 19104

**Russell J. Composto**

Department of Materials  
Science and Engineering,  
University of Pennsylvania,  
Philadelphia, PA 19104

**David M. Eckmann**<sup>2</sup>

Department of Anesthesiology and Critical Care,  
University of Pennsylvania,  
Philadelphia, PA 19104  
e-mail: eckmannm@uphs.upenn.edu

*Nanogels (NG) hold great promise as a drug delivery platform. In this work, we examine the potential of lysozyme-dextran nanogels (LDNG) as drug carriers in vitro using two cell lines: a model target tissue, human umbilical cord vein endothelial cells (HUVEC) and a model of the mononuclear phagocyte system (phorbol 12-myristate 13-acetate (PMA)-stimulated THP-1 cells). The LDNG (~100 nm) were prepared with rhodamine-label dextran (LRDNG) via Maillard reaction followed by heat-gelation reaction and were loaded with a fluorescent probe, 5-hexadecanoylamino fluorescein (HAF), as a mock drug. Epifluorescence microscopy confirmed rapid uptake of LRDNG by HUVEC. Although LysoTracker Green staining indicated a lysosomal fate for LRDNG, the mock drug cargo (HAF) diffused extensively inside the cell within 15 min. Flow cytometry and confocal microscopy indicated slow uptake of LRDNG in PMA-stimulated THP-1 cells, with only 41% of cells containing LRDNG after 24 h exposure. Finally, 24 h exposure to LRDNG did not affect the viability of either cell type at the dose studied (20 µg/ml). At a higher dose (200 µg/ml), LRDNG resulted in a marked loss of viability of HUVEC and THP-1, measuring 30% and 38%, respectively. Collectively, our results demonstrate the great potential of LRDNG as a drug delivery platform, combining simple production, rapid uptake and cargo release in target cells with “stealth” properties and low cytotoxicity. [DOI: 10.1115/1.4023246]*

*Keywords: nanogel, dextran, lysozyme, drug delivery, HUVEC, THP-1*

## Introduction

The versatility of NG makes them ideal candidates for drug delivery and bioimaging [1]. NG, often characterized as soft nanoparticles, are hydrophilic 3D networks that can absorb large amounts of water or biological fluids while maintaining their structure. In the swollen state, the low surface tension between the fluid and the NG minimizes nonspecific interactions, such as protein and cell adhesion, enhancing biocompatibility. In addition, the sub-micrometer size of the nanogels ensures that most nanogels are able to be taken up by cells, while their large surface area allows for tailoring to various *in vitro/vivo* applications and rapid responses to environment stimuli [2].

Research on drug delivery applications has mostly focused on core-shell NG. Generally, a hydrophilic shell stabilizes the NG in water/biological fluid and provides the NG with a “stealth” property, allowing them to avoid mononuclear phagocytic system (MPS) recognition as well as opsonization. The hydrophobic core allows for loading of cargo/drug via hydrophobic and electrostatic interactions. Polymers frequently used to prepare NG include polyethylene glycol-poly(ethylene imine) [3], poly(4-vinylpyridine)-poly(N-isopropylacrylamide) [4], and natural polymers. The use of polysaccharides, such as dextran, for the hydrophilic shell is particularly appealing for biomedical applications due to well-documented biocompatibility and biodegradability, multiple reactive sites for attachment of specific ligands, and steric protection against protein adsorption [5–13].

Common synthesis methods to prepare core-shell NG include (inverse) emulsion polymerization [14], precipitation polymerization [15], and photopolymerization [16]. Alternatively, core-shell NG can be prepared via two simple steps, Maillard reaction and

heat gelation. The Maillard reaction is a natural nontoxic reaction that links a protein and a polysaccharide. Subsequent heat gelation ensures partial denaturation of the protein and stable formation of the NG. This technique has several notable advantages: it is low-cost, completely “green” (i.e., it takes place in an aqueous solution) and initiator-free. Following this methodology, Li et al. synthesized NG with a LDNG that could be tailored from 80 nm to 1 µm in diameter [7]. In particular, LDNG (200 nm diameter) were spherical in shape, stable across a broad range of pH values and ionic strength, and capable of loading ibuprofen. Similar methodology has been used to prepare other protein-polysaccharide core-shell NG, such as bovine serum albumin (BSA)-dextran [9], BSA-dextran-chitosan [17], and doxorubicin-BSA-dextran [18] core-shell nanoparticles. The latter NG was found to prolong the life of mice having hepatoma H22 tumors [18].

In this work, we prepare rhodamine-labeled LDNG (LRDNG) and demonstrate their potential for use as carriers for drug delivery. This was accomplished by loading a fluorescent molecular probe (HAF) into the core of the LRDNG to model a drug. HUVEC were used as a cell culture model to verify the uptake of the LRDNG and drug release, as well as to assess cytotoxicity. Finally, the “stealth” characteristics of the LRDNG were confirmed using differentiated macrophages (PMA-stimulated THP-1 cells), as a model for the MPS.

## Materials and Methods

**Materials.** Rhodamine B isothiocyanate–Dextran (RDEX) from *Leuconostoc* ssp. (64–76 kDa molecular weight), lysozyme from chicken egg white, sodium hydroxide, silver nitrate, and all other chemical reagents were purchased from Sigma-Aldrich (St. Louis, MI) unless otherwise stated. Hanks balance salt solution (HBSS) and molecular probes 5-hexadecanoylamino fluorescein (HAF), LysoTracker Green, CellTrace™ Calcein Violet AM, and

<sup>1</sup>These authors contributed equally to this work.

<sup>2</sup>Corresponding author.

Manuscript received September 11, 2012; final manuscript received December 10, 2012; published online July 11, 2013. Assoc. Editor: Malisa Sarntinoranont.

alamarBlue<sup>®</sup> were purchased from Invitrogen (Carlsbad, CA). Primary HUVEC were purchased from Life Line Cell Technologies (Watersville, MD). Human monocyte derived macrophage cell line (THP-1) stably transduced with green fluorescent protein (GFP) actin was obtained from Dr. Stanley Stachelek (The Children's Hospital of Philadelphia, PA) [19]. Millipore water (18.2 MΩ cm) was used.

**Instruments.** The particle size and size distribution of the hydrated LRDNG (diluted 10 x) was determined by dynamic light scattering using a ZS90 Malvern Zetasize Nano series instrument (Malvern, Westborough, MA) equipped with a 22 MW He-Ne laser operating at a wavelength of 633 nm. UV spectra of LRDNG solution (diluted 10 x) were recorded on a Cary 5000 UV-vis-NIR spectrophotometer (Varian, Inc., Palo Alto, CA). LRDNG morphology was imaged by transmission electronic microscopy (TEM) on a JEM 2010 (JEOL, Ltd., Peabody, MA) at 80 kV. The samples were prepared by placing a dilute drop of the LRDNG solution onto a holey carbon TEM grid (Structure Probe, Inc., West Chester, PA). Excess liquid was removed via capillary action using a paper filter at the bottom of the TEM grid. TEM micrographs were analyzed using ImageJ (NIH, Bethesda, MD). Epifluorescence microscopy was performed using an Olympus IX70 microscope (Olympus, Melville, NY) outfitted with a Chroma Photofluor metal halide light source (89 North, Burlington, VT). Images were captured using a SensiCam QE camera (The Cooke Corp., Romulus, MI) (2 × 2 binning, 688 × 520). IPLAB software was used for image acquisition and to control the LUDL programmable filter wheels, shutters, and focus (Ludl Electronic Products, Hawthorne, NY). Confocal microscopy was performed on an Olympus IX81 with Fluoview FV1000 controller. Fluoview 1.6 was used for image acquisition and ImageJ was used for analysis. Plate reader assays were performed using CHAMELEON<sup>™</sup> V (Hidex, Turku, Finland). Flow cytometry was performed using BD FACSCalibur and CellQuest software (Becton Dickinson, San Jose, CA). Two-color analysis was performed with FlowJo software (Tree Star, Inc., OR).

**Synthesis of LRDNG.** The synthesis of LRDNG was adapted from previous reported studies [7,20]. Briefly, RDEX from *Leuconostoc* ssp. and lysozyme were dissolved (1:1) in water, the pH was adjusted to 7–8 using 0.1 N sodium hydroxide, and the solution was lyophilized. The lyophilized powder was allowed to react at 60 °C under 79% relative humidity in a desiccator containing saturated KBr solution for 18–24 h. The reacted powder was dissolved in water (5 mg/ml), the pH was adjusted to 10.7 using 0.1 N sodium hydroxide, and the solution was further reacted at 80 °C for 30 min. The resulting LRDNG was allowed to cool down to room temperature and were purified by centrifugation using Amicon Ultra-0.5 ml centrifugal filter devices with a 100 kDa molecular weight cutoff (Millipore, Billerica, MA), following the directions of the manufacturer (14,000xg for 12 min for reactant removal and 1000xg for 2 min for LRDNG retentate recovery). The purified LRDNG were stored in the dark at 4 °C. The LRDNG efficiency was estimated by measuring the absorbance of lysozyme present in the retentate and filtrate at 280 nm.

**Loading of LRDNG With a Mock Drug.** Stock solutions of HAF were prepared in ethanol at a final concentration of 60 μg/ml, 6 mg/ml, and 60 mg/ml and stored at 4 °C. LRDNG (5 mg/ml) were incubated with HAF at a final concentration of 20 ng/ml, 0.12 mg/ml, and 1.2 mg/ml for at least 3 days at 4 °C (HAF-LRDNG). Before use, HAF-LRDNG were centrifuged to remove free HAF. The HAF loading amount and efficiency was estimated by comparing the initial HAF in the loading solution with the LRDNG filtrate at 520 nm to a known calibration curve using a Fluorolog spectrofluorometer (Horiba Scientific, Edison, NJ).

**Endothelial Cell Culture.** HUVEC were cultured in VascuLife VEGF Cell Culture Media (Lifeline Cell Technology,

Walkersville, MD). Media samples were regularly checked for mycoplasma contamination using MycoAlert Kit (Lonza, Rockland, ME). For all experiments, cells between passage 2 and 6 were plated onto 35 mm MatTek glass bottom cell culture dishes (MatTek Co., Ashland, MA) coated with 2 μg/cm<sup>2</sup> fibronectin at a density of 5000 cells/cm<sup>2</sup>. Prior to experiments, the cells were allowed to grow for 48–72 h. All fluorescence imaging and assays were carried out at room temperature in HBSS, pH 7.4 with 1.3 mmol/l CaCl<sub>2</sub>, 0.9 mmol/l MgCl<sub>2</sub>, 2 mmol/l GlutaMax, 10 g/l heparin, 5.6 mmol/l glucose, and 1% FBS).

**Imaging of HAF-LRDNG in HUVEC.** On the day of a given experiment, the cell culture media was replaced with 20 μg/ml HAF-LRDNG suspension in media. As a control, the experiment was also performed with HBSS instead of HAF-LRDNG suspension. After 1, 3, 6, and 24 h of incubation with HAF-LRDNG, the cells were washed with sterile HBSS three times (1 ml) to remove any residual LRDNG and imaged using epifluorescence microscopy. As a control for the extracellular release of HAF from the HAF-LRDNG, the experiments were repeated with 2.5 ml of HAF-LRDNG dialyzate, instead of HAF-LRDNG suspension. Briefly, 4 ml of HAF-LRDNG at 100 μg/ml were diluted with 6 ml of cell culture media and dialyzed against 10 ml of cell culture media using a semipermeable, regenerated cellulose dialyzing tubing (MW cutoff 15 kDa, Spectrum Labs) for 1, 3, 6, and 24 h. The cells were subsequently imaged, and data were compared to cells treated with the HAF-LRDNG suspension. The data represents the means of two independent experiments performed in quinticates.

In order to confirm intracellular HAF delivery, HUVEC were treated with 20 μg/ml HAF-LRDNG suspension for 15 min at 37 °C, followed by three washes with HBSS (1 ml) to remove any residual LRDNG. In parallel, as a control for extracellular HAF release, the HAF-LRDNG suspension was incubated without cells for 15 min at 37 °C, followed by centrifugation using Amicon Ultra-0.5 ml centrifugal filter devices with a 100 kDa molecular weight cutoff. HUVEC were then incubated with the resulting filtrate for 15 min at 37 °C, followed by three washes. Treated cells were then imaged using epifluorescence microscopy and the signal was compared to cells exposed to a HBSS control.

**Intracellular Fate of LRDNG in HUVEC.** HUVEC were cultured and exposed to LRDNG as described previously. Prior to imaging, the cells were incubated with LysoTracker Green at a concentration of 75 nM in HBSS for 1 h at 37 °C and then washed. Confocal microscopy was used to collect z-stacks of individual cells, 0.5 μm per slice. Slices were scanned sequentially to minimize bleed through and cross talk. Analysis of colocalization was performed on entire stacks, using the Costes method [21] as implemented in the Colocalization Threshold plugin (Wright Cell Imaging Facility, Toronto, Canada) for ImageJ. The images are representative of two independent experiments performed in duplicate.

**THP-1 Cell Culture.** THP-1 cells, stably transduced with GFP-actin, were maintained in suspension culture in RPMI media (Gibco, Grand Island, NY), supplemented with 10% FBS (HyClone, Rockford, IL), 1% penicillin streptomycin (Invitrogen, Carlsbad, CA), and 0.05 mM 2-mercaptoethanol. For all experiments, GFP-actin THP-1 cells (25,000 cells/cm<sup>2</sup>) were stimulated to differentiate into adherent macrophages on 35 mm MatTek glass bottomed cell culture dishes (MatTek Co, Ashland, MA) with the addition of 1 μg/ml of PMA for 72 h.

**Imaging of LRDNG in PMA-Stimulated THP-1 Cells.** Cells were cultured and exposed to HAF-LRDNG as described previously. After 24 h of incubation with LRDNG, the cells were washed with HBSS three times (1 ml) to remove any residual LRDNG. For imaging, 1 ml of cell culture media was added to

each dish. The images are representative of two independent experiments performed in triplicate.

**Flow Cytometry of PMA-Stimulated THP-1 Cells Exposed to LRDNG.** Phagocytosis of LRDNG by PMA-stimulated, GFP-actin THP-1 cells (FL-1) was determined after 1, 3, 6 and 24 h of incubation with the LRDNG (FL-2) via flow cytometry. Cells were cultured and exposed to LRDNG as described previously. Following LRDNG exposure, cells were scraped using a cell scraper and transferred into FACs tubes. Mean GFP fluorescence was calculated from 50,000 live cells per sample. Cells that may have clumped together were gated out based on their forward and side scatter profiles. Fluorescence minus one test was used to identify the true-negative population for rhodamine fluorescence ( $10^2$ ).

**Viability of HUVEC.** The viability of HUVEC after exposure to the LRDNG for 24 h at various concentrations was determined by quantifying the reduction of the fluorogenic indicator alamarBlue. HUVEC (2000 cells per well) were allowed to attach in clear bottom, black 96-well ViewPlates (PerkinElmer, Waltham, MA). After 3 days of culture, LRDNG suspensions in media, ranging from 0 to 200  $\mu\text{g}/\text{ml}$ , were added to each well. HBSS was used as a control. After 24 h incubation, the cell culture media was refreshed with 10% alamarBlue and cells were incubated for 1 h at 37 °C, in the dark. Fluorescence was determined with a Hidex plate reader. The data are means of two independent experiments performed in triplicate.

**Viability of PMA-Stimulated THP-1 Cells.** The viability of PMA-stimulated THP-1 cells exposed to LRDNG for 24 h at various concentrations was determined by hydrolysis of an acetoxy-methyl ester derivative fluorescent indicator, Calcein Violet AM. Cells were cultured as described previously and exposed to LRDNG suspensions in media (0–200  $\mu\text{g}/\text{ml}$ ) for 24 h. HBSS was used as a control. After 24 h, the cells were loaded with 500 nm of Calcein Violet AM for 30 min at 37 °C, followed by HBSS wash. For each condition, 9 images were collected using 10x objective and viable cells were counted using ImageJ (NIH, Bethesda, MD). This experiment was performed in triplicate.

**Statistical Analysis.** Data are presented as mean  $\pm$  standard deviation, unless otherwise noted. Statistical significance between two groups was assessed via t-test, while multiple groups were compared via ANOVA followed by Dunnett's test (OriginLab, Northampton, MA). Values of  $p < 0.05$  were considered statistically significant.

## Results

**Synthesis and Characterization of LRDNG.** Fluorescently labeled nanogels based on RDEX and lysozyme were prepared following a two-step heating process [7]. First, RDEX-lysozyme conjugates were synthesized via Maillard heating reaction. Amino groups from the lysozyme were reacted with terminal carbonyl groups of the dextran in a potassium bromide saturated atmosphere. Second, LRDNG were produced via heat-gelation reaction. The RDEX-lysozyme conjugates in aqueous solution were heated above the denaturation temperature of secondary and tertiary structure of the lysozyme (80 °C) at the isoelectric point (pI) of the protein. The efficiency of LRDNG formation was 86 wt. % relative to lysozyme.

The size distribution of the LRDNG in an aqueous environment at pH 7 was measured by DLS, yielding a hydrodynamic diameter of  $107 \pm 26$  nm as shown in Fig. 1(a). The narrow Gaussian fit indicates uniform and dispersed LRDNG, which remained stable when stored for at least 6 months at 4 °C (Fig. 1(a)). Additionally, the LRDNG were serum-stable, as no significant aggregation/

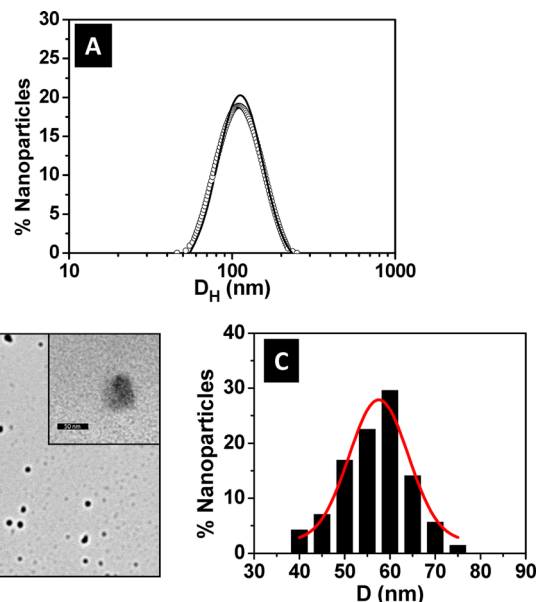


**Fig. 1** Characterization of LRDNG. (a) Size distribution as measured by DLS following synthesis (line) and after 6 month storage at 4 °C (open circles). (b) TEM micrographs showing particles after drying on holy carbon grid. The scale bars correspond to 0.5  $\mu\text{m}$  and 50 nm (inset). (c) Histogram of particle size distribution as measured from TEM micrographs. The hydrodynamic diameter ( $D_H$ ) of the LRDNG is  $107 \pm 26$  nm whereas the average particle size in the dried state (d) is  $57 \pm 13$  nm.

agglomeration was observed via DLS after 24 h, room temperature incubation with 25%, 50%, or 100% FBS (data not shown).

The morphology of the LRDNG was also imaged by TEM. The TEM micrograph presented in Fig. 1(b) shows round and well-dispersed LRDNG. The LRDNG size ranged from  $\sim 40$  to  $\sim 75$  nm in diameter as shown in Fig. 1(c). The peak diameter of the LRDNG, obtained by measuring 140 NG and fitting a Gaussian curve to the NG distribution, was  $57 \pm 13$  nm.

**Cytotoxicity of LRDNG.** The cytotoxicity of the LRDNG towards HUVEC (alamarBlue assay) and PMA-stimulated, GFP-actin THP-1 cells (Calcein Violet cell counting) was assessed following 24 h incubation of cells with LRDNG, at concentrations up to 200  $\mu\text{g}/\text{ml}$ . The percentage of viable cells, relative to control, is presented in Fig. 2. LRDNG do not appear to be cytotoxic to HUVEC (Fig. 2(a)) or THP-1 cells (Fig. 2(b)) at concentrations up to 20  $\mu\text{g}/\text{ml}$ ; however, at a LRDNG concentration of 200  $\mu\text{g}/\text{ml}$  we observed a marked reduction in viability of both cell types (30% for HUVEC and 38% for THP-1 cells).

**Loading of NG With a Mock Drug.** As a proof of concept simulating the loading of a drug, the LRDNG were loaded with a fluorescent molecular probe, HAF. The amphiphilic properties of HAF ensured diffusion of HAF into the interior interface of the NG formed by the less hydrophilic lysozyme core and the RDEX shell. To guarantee complete saturation of LRDNG with HAF, the LRDNG (5 mg/ml) were incubated with HAF for 3 days with HAF after which the excess of HAF was eliminated via centrifugation. Figure 3 illustrates the loading amount, defined as the weight ratio of loaded HAF to LRDNG, and the loading efficiency, defined as the weight ratio of loaded HAF to initial HAF, for the different HAF concentrations studied as estimated by fluorescence measurements. Increasing the initial loading concentration of HAF from 20 ng/ml to 1.2 mg/ml resulted in an increase in the amount loaded from 0.004 wt. % to 3 wt. %, respectively. However, the highest loading amounts, 0.93 wt. % and 3 wt. % suffer from inferior loading efficiencies of 33% and 11%,

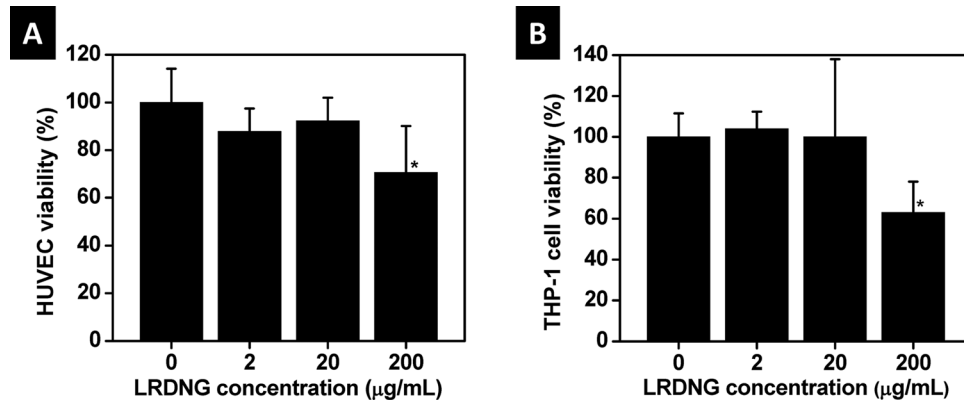


Fig. 2 Viability of cells after 24 h exposure to a range of LRDNG concentrations. (a) Viability of HUVEC, determined using alamarBlue<sup>®</sup> indicator. (b) Viability of PMA-stimulated, GFP-actin THP-1 cells, determined using Calcein Violet. \* indicates significant difference from control,  $p < 0.05$ .

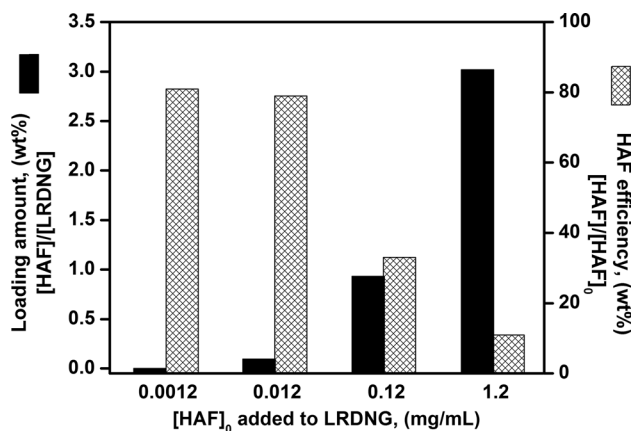


Fig. 3 Summary of loading amount, defined as the weight ratio of loaded HAF to LRDNG ( $[HAF]/[LRDNG]$ ) and loading efficiency, defined as the weight ratio of loaded HAF to initial HAF ( $[HAF]/[HAF]_0$ ) as a function of the loading concentration

respectively. For all the cell uptake studies described below, LRDNG with 0.004 wt. % HAF were employed, as this amount was found to be optimal for fluorescence imaging studies.

**HUVEC Uptake of LRDNG and Release of the Mock Drug.** In these studies, we used epifluorescence microscopy to assess fluorescence intensity as a quantitative measure of cellular

uptake of HAF-LRDNG and release of HAF drug. Figure 4(a) shows a representative epifluorescence photomicrograph of cells treated with 20 μg/ml of LRDNG (red) loaded with the mock drug, HAF (green), for 1 h. The relative fluorescence intensities of the LRDNG and HAF as functions of incubation time of HUVEC with HAF-LRDNG are summarized in Figs. 4(b) and 4(c), respectively. Our results indicate that after incubation of cells with HAF-LRDNG for 1 h, cellular uptake occurred in all cells and the intracellular amount of HAF-LRDNG was measurable. As the incubation time increased, the amount of HAF-LRDNG taken by the cell increased, peaking at 6 h incubation time. A similar trend was observed for the intracellular release of HAF; intracellular HAF release increased with HAF-LRDNG incubation time, up to 6 h and then remained steady after 24 h incubation.

To ensure the release of HAF mock drug measured was from HAF-LRDNG inside the cell, the HAF fluorescence released from the HAF-LRDNG outside the cells was also assessed. To do so, HAF-LRDNG were dialyzed against HBSS at the different incubation times studied and these dialyzates were then used to treat HUVEC at their corresponding incubation times. The fluorescence intensity measured from HUVEC treated with the dialyzate from HAF-LRDNG outside the cells is shown in Fig. 4(c). Free HAF released from HAF-LRDNG was insignificant at 1 and 3 h HAF-LRDNG incubation time (i.e., less than 0.5% of the incorporated HAF leached out), indicating that the HAF detected in the cells was due to HAF released from intracellular HAF-LRDNG. However, at higher HAF-LRDNG incubation times, the free HAF released from the HAF-LRDNG increased and accounted for 19% and 32% of the total HAF uptake by the cells at 6 h and 24 h

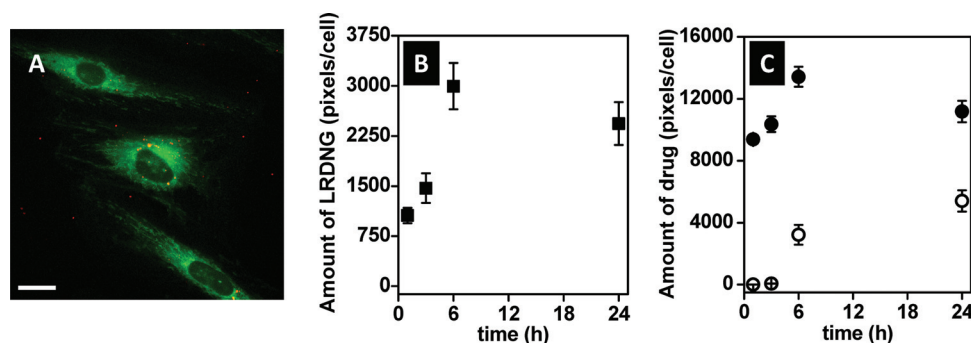
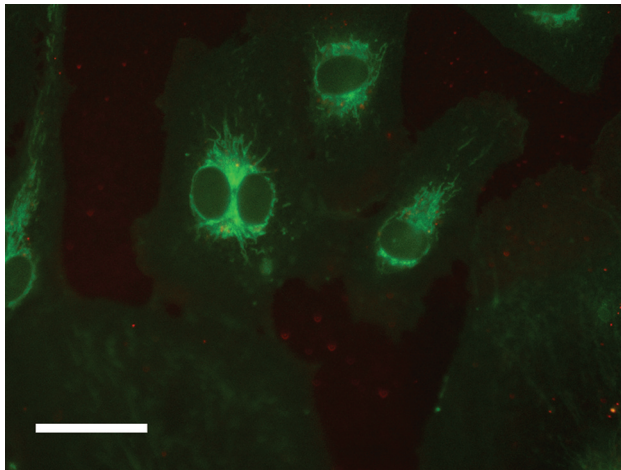


Fig. 4 HUVEC uptake of HAF-LRDNG by epifluorescence microscopy. (a) Representative epifluorescence photomicrograph of cells after 1 h incubation with LRDNG (red) loaded with mock drug, HAF, (green), namely HAF-LRDNG. The scale bar corresponds to 10 μm. (b) Uptake of HAF-LRDNG and (c) intracellular (closed circles) and extracellular (open circles) release of mock drug HAF as a function of incubation time.



**Fig. 5** HUVEC uptake of HAF-LRDNG and intracellular HAF release after 15 min by epifluorescence microscopy. Representative epifluorescence photomicrograph of cells after 15 min incubation with LRDNG (red) loaded with mock drug, HAF, (green), namely HAF-LRDNG. The scale bar corresponds to 20  $\mu\text{m}$ .

incubation time. These amounts have been subtracted accordingly in the results shown in Fig. 4(c) (closed squares).

We further confirmed intracellular HAF release by treating HUVEC with 20  $\mu\text{g}/\text{ml}$  HAF-LRDNG suspension for 15 min at 37  $^{\circ}\text{C}$ . Alternatively, as a control for extracellular HAF release, HUVEC were treated with the filtrate of a HAF-LRDNG suspension incubated without cells for 15 min at 37  $^{\circ}\text{C}$ , followed by centrifugation using Amicon Ultra-0.5 ml centrifugal filter devices with a 100 kDa molecular weight cutoff. Figure 5 shows a representative epifluorescence photomicrograph of cells treated with 20  $\mu\text{g}/\text{ml}$  of LRDNG (red) loaded with the mock drug, HAF (green), for 15 min. We observed a strong green staining pattern, consistent with HAF staining of intracellular membrane-rich compartments, such as mitochondria. Diffuse green fluorescence throughout the cell likely indicates a combination of HAF still present inside LRDNG and HAF bound to the plasma membrane. Additionally, we observed weak red and green signal outside cells, indicating some adsorption of the HAF-LRDNG to the fibronectin-coated glass. No significant difference in fluorescence was observed between cells treated with HAF-LRDNG filtrate or HBSS control ( $177 \pm 1.3$  A.U. versus  $180 \pm 1.6$  A.U.,  $p=0.92$ ,  $N=3$ ), confirming that extracellular HAF leakage from HAF-LRDNG was negligible over the course of 15 min.

**Localization of the LRDNG and Mock Drug in HUVEC.** In order to determine the intracellular fate of the LRDNG, HUVEC were stained with LysoTracker Green following exposure to HAF-LRDNG for 1 h and imaged via confocal microscopy. Figure 6 shows a representative confocal slice of LRDNG uptake in HUVEC, with white highlighting indicating colocalization between NG and lysosomes as determined by the Costes image analysis. NG can be seen distributed throughout the cell, as well as clustered in lysosomes. The volumetric image analysis of colocalization in 5 cells indicates that  $17 \pm 8\%$  of the above threshold LRDNG fluorescence intensity originates from voxels above the LysoTracker Green threshold, as determined by the Costes analysis. These findings indicate a lysosomal fate for the LRDNG.

**Uptake of LRDNG by PMA-Stimulated, GFP-Actin THP-1 Cells.** The uptake of the LRDNG by PMA-stimulated, GFP-actin THP-1 cells was determined by confocal microscopy. To ensure complete removal of particles adhered to the cell surface, the cells were rinsed three times with HBSS after the incubation set times.

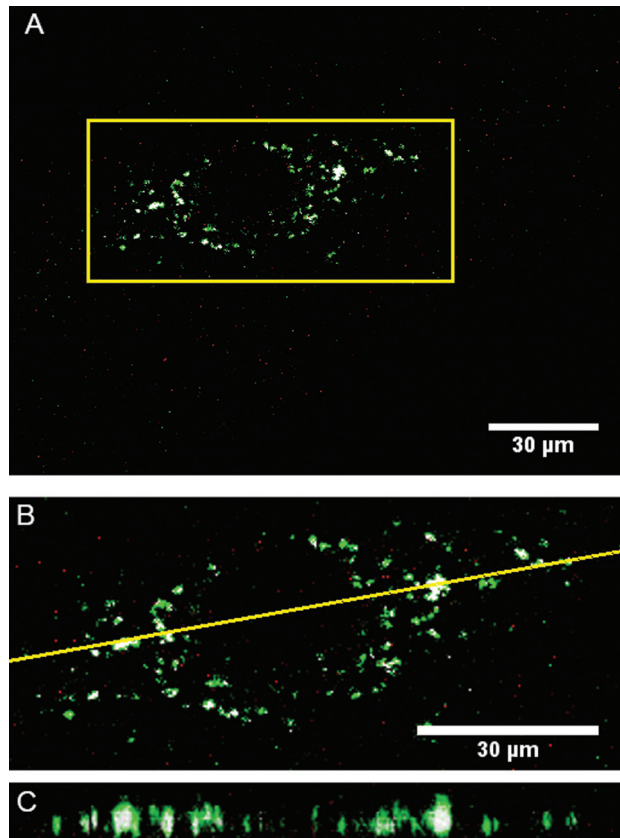


**Fig. 6** Localization of LRDNG (red) inside HUVEC after 1 h. RDNG are pseudocolored red, lysozymes are pseudocolored green, and colocalization, as determined by the Costes image analysis, is highlighted in white. (a) Single, middle confocal slice of a representative cell. (b) Zoomed in view of the region highlighted in panel A. (c) XZ rendering for the plane indicated by the yellow line in panel B.

Figure 7(a) shows a representative middle slice of confocal z-stack of PMA-stimulated, GFP-actin THP-1 cells following 24 h exposure to the LRDNG, indicating that cellular uptake did not occur in all cells after 24 h. A 3D image of an individual PMA-stimulated, GFP-actin THP-1 cell with internalized LRDNG following 24 h exposure to LRDNG is shown in Figs. 7(b) and 7(c) is a plot indicating the sum of fluorescence intensity of green (GFP-actin) and red (LRDNG) channels for all z heights ( $0.2 \mu\text{m}$  step size) in the corresponding 3D image shown in Fig. 7(b). The green fluorescence corresponds to the cytoskeleton of the cell (GFP-actin) and indicates the cell topography, showing an increase in intensity near the nucleus, in agreement with the thickness of the cell. The red fluorescence of the LRDNG is within the limits of the green fluorescence intensity confirming that the LRDNG are not on the cell surface, but internalized.

The phagocytosis of LRDNG by PMA-stimulated, GFP-actin THP-1 cells was studied over time using flow cytometry. Figure 8 shows the histograms of control cells and cells incubated with the LRDNG for 1 h, 3 h, 6 h, and 24 h, as well as a summary of cellular uptake versus incubation time (Fig. 8(f)). Gating was performed around the control population of cells not incubated with LRDNG. The FL-1 channel indicates GFP-actin fluorescence (green), while the FL-2 channel indicates LRDNG fluorescence (red). After incubation of the LRDNG for 1 h (Fig. 8(b)), 0.68% of the cells demonstrate increased red fluorescence, indicating internalized LRDNG, as compared to 0.26% of the control cells (Fig. 8(a)). With increased LRDNG incubation time up to 3 h (Fig. 8(c)) and 6 h (Fig. 8(d)), a linear increase in the percentage of cells with internalized LRDNG was observed, reaching 8% and

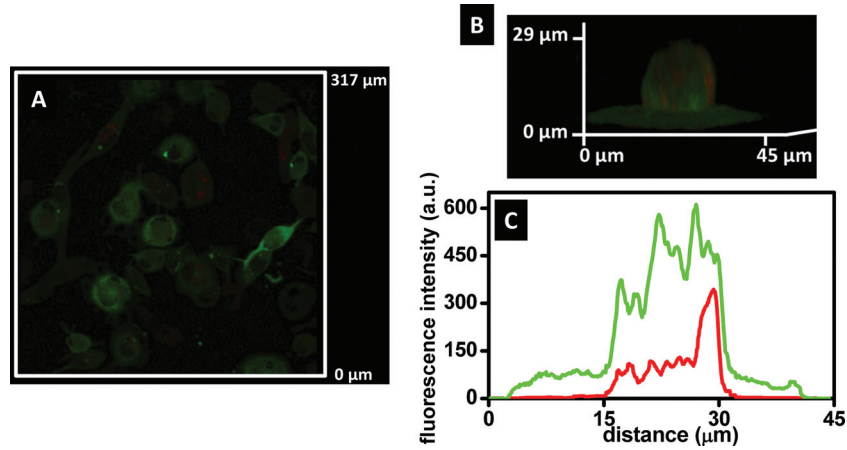


**Fig. 7 Uptake of LRDNG by PMA-stimulated, GFP-actin THP-1 cells by confocal microscopy following 24 h incubation. (a) Representative epifluorescence photomicrograph of middle slice of confocal z stacks (b) 3D image of a single cell. (c) Sum of fluorescence intensities of green (GFP-actin) and red (LRDNG) channels for all z heights (0.2  $\mu\text{m}$  steps) of the 3D image, indicating LRDNG inside the cell body and not on the surface.**

20% at 3 and 6 h incubation time, respectively. However, after 24 h incubation with LRDNG (Fig. 8(e)), only 41% of cells had internalized LRDNG.

## Discussion

Recent advances in nanotechnology have shown great potential to revolutionize medicine and drug delivery, in particular. However, despite tremendous progress and promise shown in the lab, the translation of this research to the clinic is still a work in progress [22]. For a drug delivery platform to successfully translate into the clinical setting, it needs to possess an optimal combination of straightforward and reproducible preparation, biocompatibility (both lack of toxicity, as well as “stealth”), stability, and ability to both load and unload cargo.

In this work, we have examined for the first time the potential of LRDNG as drug carriers *in vitro*. LRDNG were successfully prepared following two simple steps: Maillard reaction, followed by heat-gelation reaction. This “green” methodology (i.e., aqueous solution, initiator-free) ensures the formation of a core-shell type nanogel, with a protein-rich (lysozyme) core and a polysaccharide-rich shell (dextran) [7]. The more hydrophilic dextran stabilizes the lysozyme, a polar protein with hydrophobic moieties, which otherwise would aggregate in solution [23].

We chose to focus on LDNG, because of their high stability and neutral behavior within  $pH$  2–12 [7]. This advantage was not observed in other NG prepared using similar methodology, BSA-dextran [9] or BSA-dextran-chitosan [18] NG. Further, the presence of partially denatured lysozyme in the LDNG may provide an antibacterial effect versus some bacterial strains [24] and

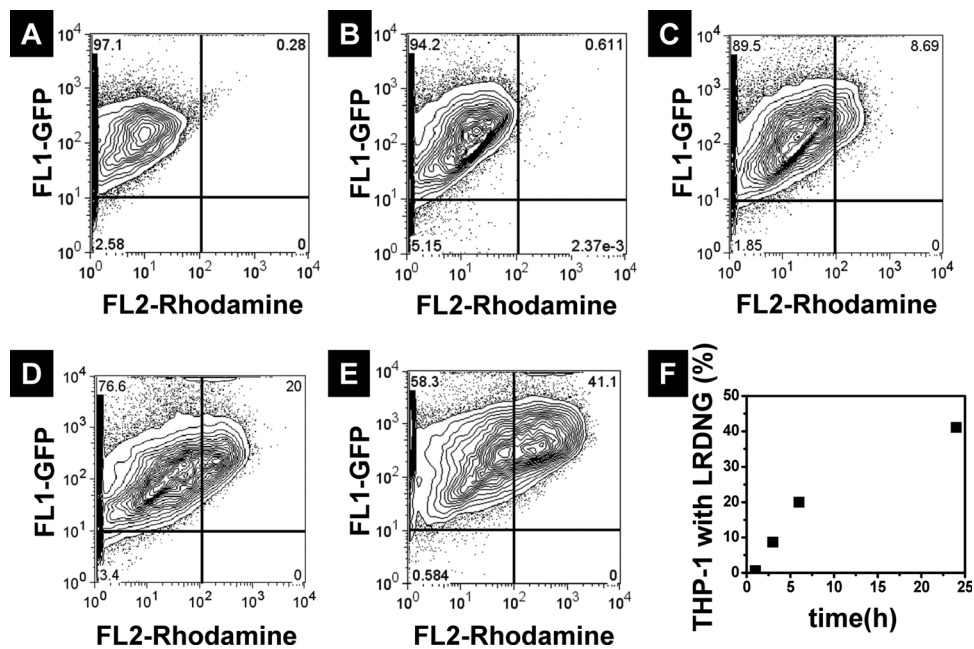


**Fig. 8 Flow cytometry analysis of LRDNG uptake by PMA-stimulated, GFP-actin THP-1 cells. Histograms of (a) control cells and cells incubated with LRDNG for (b) 1 h, (c) 3 h, (d) 6 h, and (e) 24 h. (f) Summary of percentage of cells containing LRDNG as a function of incubation time.**

thereby have utility as an anti-infective agent. Meanwhile, dextran, an  $\alpha(1-6)$ -linked glycan, is nontoxic, water soluble and neutral, with multiple reactive sites available for subsequent functionalization for targeting ligands. Importantly, dextran has demonstrated outstanding properties against nonspecific protein adhesion by our group [25,26] and others [27–29]. Finally, dextran coated delivery systems have shown both reduced opsonisation by proteins in the medium [30] and reduced nonspecific hydrophobic interactions between the carrier and cell membranes. Examples of dextran coated carriers include liposomes [31–33], polymeric micelles [34–36], and nanogels [7,37,38]. The latter carriers are particularly important because they allow for higher drug encapsulation and protection. Among them, we chose the NG platform because it is designed to yield a drug carrier that is nontoxic, stable, and “stealthy.”

Here, for the first time, the LDNG were prepared using fluorescently labeled dextran, Rhodamine B isothiocyanate–Dextran, which provides a label for following cellular uptake of the NG by fluorescence microscopy. Using RDEX produced LRDNG with a diameter of 100 nm. The LRDNG were well-dispersed, as indicated by the narrow size distribution measured by DLS and as observed by TEM. In contrast to previously reported LDNG using similar conditions [20], our LRDNG were approximately 50% smaller in size. Rhodamine B isothiocyanate is a hydrophobic molecule and therefore increases the hydrophobicity of dextran, even though the extent of labeling of RDEX was very low (1–7 rhodamine B isothiocyanate molecules per dextran chain). As a result, the hydrophobic fluorophore molecules are more likely to penetrate into the lysosome core, resulting in tighter, smaller NG. The LRDNG swelled approximately sevenfold in aqueous solution (as estimated by comparing DLS with TEM data), allowing room for storage of amphiphilic/hydrophobic drug cargo. Comparable swelling was observed in LDNG (data not shown), indicating that both have similar dextran to lysosome content ratio. Further, because TEM is a 2D technique and LRDNG in the dried state acquire an ellipsoidal shape, the actual swelling is likely to be even greater. Importantly, the LRDNG remained stable in solution for over six months when stored at 4 °C (Fig. 1(a)) and were stable in serum for at least 24 h. As a proof of concept, we were able to successfully load our LRDNG with a mock drug, HAF, via hydrophobic/electrostatic interactions. HAF, C<sub>16</sub>-palmitoyl-modified fluorescein, is a lipophilic dye that mimics bioactive lipids or other drugs which are poorly water soluble. The choice of HAF allows us to visualize the unloading of cargo inside live cells, as extracellular free dye is poorly internalized and primarily stains the apical plasma membrane [39,40].

As drug delivery vehicles, targeted NG (and nanoparticles in general) are an ideal drug delivery vehicle for intravenous applications, as has been extensively described in the literature [1,2]. NG provide the means to work around solubility issues, poor cellular uptake, and off-target toxicity. Clearly, NG must be able to be taken up by target cells (with minimal cytotoxicity) and release drug cargo. We selected endothelial cells as our *in vitro* target cell because the endothelium is an important target for vascular drug delivery, given its involvement in angiogenesis, atherosclerosis, tumor growth, etc. Further, HUVEC in particular have been well characterized and extensively used in the field of vascular biology [41]. As a successful clinical drug delivery platform, it is also important that NG not be cleared by mononuclear phagocyte system, which would not only reduce the effective dose at the target tissue, but possibly cause immunological complications. Thus, it is important to assess the interactions between NG and the immune system [42]. In this work, we used THP-1 cells (a monocytic cell line) and THP-1 cells stimulated with PMA, which serves to differentiate them into adherent macrophages [43], as *in vitro* models of the MPS.

First, we assessed the cytotoxicity of the LRDNG in both cell culture models. Exposure of cells to LRDNG concentrations up to 20  $\mu\text{g}/\text{ml}$  for 24 h did not result in any significant cytotoxicity. The maximum concentration used, 200  $\mu\text{g}/\text{ml}$ , did result in a

marked reduction in cell viability in both cell types, however this LRDNG concentration in the blood would be analogous to a dose of approximately 15 mg/kg in a human, which is greater than the typical dose of many pharmaceutical agents. Thus, we anticipate that at typical dosages, LRDNG will prove nontoxic and safe for drug delivery applications.

Our results indicate that HAF-LRDNG are rapidly taken up by endothelial cells in culture (Fig. 4) when exposed to a stable dispersion of HAF-LRDNG. Within an hour, LRDNG are already visible inside cells. However, the actual uptake is likely to be much faster, because individual LRDNG are smaller than the resolution limit of our microscope objective and, thus, the much of red fluorescence observed after 1 h likely represents LRDNG that cluster inside cells. In fact, we observe robust HAF staining of intracellular membranes (Fig. 5) following 15 min of incubation with HAF-LRDNG, while minimal clustering is observed in the red channel. These results were confirmed with confocal microscopy, which indicated that after one hour the majority of LRDNG are dispersed throughout the cell. However, LysoTracker Green staining (Fig. 6) and colocalization threshold analysis, using the costes method [21], indicates that a fraction of the LRDNG does cluster in lysosomes after 1 h exposure, suggesting that this is their ultimate fate. Over time, cellular uptake of LRDNG increases, before leveling off between 6 and 24 h. Because these LRDNG are biodegradable, at longer times the time course represents the combination of uptake, intracellular trafficking, as well as degradation of LRDNG. Rapid uptake and lysosomal fate of the LRDNG is not surprising and, given their small size (~100 nm), neutral potential, and lack of targeting ligand, is consistent with pinocytotic uptake [44]. However, the use of dextran as the shell component, which has multiple functional sites, does allow us to readily change the zeta potential or to add targeting ligands in the future. Despite the ultimate lysosomal fate of the LRDNG, fluorescence imaging of the mock drug cargo, HAF, indicates that within 15 min this small molecule has been able to access intracellular membranes within the cell (Fig. 5), indicating successful mock drug delivery by these NG. Further experiments will be needed to determine the mechanism by which the cargo is released inside the cell.

In order to assess the “stealth” characteristics of the NG, we first exposed naive THP-1 cells to LRDNG for 3 days, which did not result in any transformation, adhesion, or loss of viability (data not shown). Next, we exposed THP-1 cells stimulated with PMA, which serves to differentiate them into adherent macrophages to LRDNG in similar fashion to the endothelial cell experiments and assessed LRDNG uptake via flow cytometry. In contrast to the rapid uptake observed in all HUVEC, the PMA-stimulated THP-1 cells took up LRDNG very slowly (Fig. 8). After 1 h virtually no uptake is observed and after 24 h only 41% of cells contained LRDNG. We conclude that the LRDNG do not trigger phagocytotic uptake, despite the presence of 10% serum in the media, which could cause some opsonization. This is consistent with the previous finding that the LRDNG are serum stable and do not aggregate/agglomerate, which could also facilitate phagocytosis. Collectively, these findings confirm the “stealth” property of the LRDNG, suggesting LRDNG will not trigger adverse immunological effects and be able to circulate freely for an extended period of time.

## Conclusion

In conclusion, we have examined the viability of dextran-lysosome nanogels as a drug delivery systems using fluorescently labeled NG loaded with a fluorescent molecular probe as a mock drug in two *in vitro* models. These LRDNG show great potential, based on their lack of cytotoxicity and rapid release of the drug in HUVEC before reaching the lysosomes, as compared to their slow uptake by macrophages. Using simple modifications, these LRDNG can fulfill many desired applications; for example, LRDNG can be decorated with specific ligands on the outer

dextran shell to interact with specific receptors [45], and the biodegradability of the LRDNG can be tuned by adding enzymes such as dextranase. Furthermore, the core allows for transport of a variety of molecules/nanoparticles other than drugs, such as silver nanoparticles for antibacterial, optical and therapeutic applications [20]. Overall, these results are very promising and we plan further *in vivo* studies to fully assess the potential of LRDNG for drug delivery.

## Acknowledgment

We acknowledge the support of NIH Grant Nos. R01 HL060230 and R01 EB006818 (DME) and Penn Regional Nanotechnology Center (TEM), NSF/NBIC (RJC) and NSF Polymers Program (RJC). The authors thank Robert C. Ferrier, Jr. for imaging the TEM samples, Benjamin Pichette for imaging HAF-LRDNG in HUVEC and for carrying out HUVEC viability study, Tatyana Milovanova for performing flow cytometry analysis, Dr. Stanley Stachalek (The Children's Hospital of Philadelphia) for providing GFP-actin transduced THP-1 cells, Professor Ivan J. Dmochowski for access to confocal microscope, Liao Zhengzheng for training in confocal microscopy, and Judith Kandel for proof-reading and editing the manuscript. The authors have no conflicts of interest.

## References

- [1] Oh, J. K., Drumright, R., Siegart, D. J., and Matyjaszewski, K., 2008, "The Development of Microgels/Nanogels for Drug Delivery Applications," *Prog. Polym. Sci.*, **33**(4), pp. 448–477.
- [2] Raemdonck, K., Demeester, J., and De Smedt, S., 2009, "Advanced Nanogel Engineering for Drug Delivery," *Soft Matter*, **5**(4), pp. 707–715.
- [3] Kuckling, D., Vo, C. D., and Wohlrab, S. E., 2002, "Preparation of Nanogels With Temperature-Responsive Core and pH-Responsive Arms by Photo-Cross-Linking," *Langmuir*, **18**(11), pp. 4263–4269.
- [4] Li, X., Zuo, J., Guo, Y. L., and Yuan, X. H., 2004, "Preparation and Characterization of Narrowly Distributed Nanogels With Temperature-Responsive Core and pH-Responsive Shell," *Macromolecules*, **37**(26), pp. 10042–10046.
- [5] Lemarchand, C., Gref, R., and Couvreur, P., 2004, "Polysaccharide-Decorated Nanoparticles," *Eur. J. Pharm. Biopharm.*, **58**(2), pp. 327–341.
- [6] Mitra, S., Gaur, U., Ghosh, P. C., and Maitra, A. N., 2001, "Tumour Targeted Delivery of Encapsulated Dextran-Doxorubicin Conjugate Using Chitosan Nanoparticles as Carrier," *J. Controlled Release*, **74**(1–3), pp. 317–323.
- [7] Li, J., Yu, S. Y., Yao, P., and Jiang, M., 2008, "Lysozyme-Dextran Core-Shell Nanogels Prepared Via a Green Process," *Langmuir*, **24**(7), pp. 3486–3492.
- [8] Nagahama, K., Ouchi, T., and Ohya, Y., 2008, "Biodegradable Nanogels Prepared by Self-Assembly of Poly(L-Lactide)-Grafted Dextran: Entrapment and Release of Proteins," *Macromol. Biosci.*, **8**(11), pp. 1044–1052.
- [9] Li, J., and Yao, P., 2009, "Self-Assembly of Ibuprofen and Bovine Serum Albumin-Dextran Conjugates Leading to Effective Loading of the Drug," *Langmuir*, **25**(11), pp. 6385–6391.
- [10] Jeong, Y. I., Choi, K. C., and Song, C. E., 2006, "Doxorubicin Release From Core-Shell Type Nanoparticles of Poly(DI-Lactide-Co-Glycolide)-Grafted Dextran," *Arch. Pharmacol. Res.*, **29**(8), pp. 712–719.
- [11] Pan, X. Y., Yao, P., and Jiang, M., 2007, "Simultaneous Nanoparticle Formation and Encapsulation Driven by Hydrophobic Interaction of Casein-Graft-Dextran and Beta-Carotene," *J. Colloid Interface Sci.*, **315**(2), pp. 456–463.
- [12] Jung, S. W., Jeong, Y. I., Kim, Y. H., Choi, K. C., and Kim, S. H., 2005, "Drug Release From Core-Shell Type Nanoparticles of Poly(DI-Lactide-Co-Glycolide)-Grafted Dextran," *J. Microencapsul.*, **22**(8), pp. 901–911.
- [13] Lemarchand, C., Gref, R., Passirani, C., Garcion, E., Petri, B., Muller, R., Costantini, D., and Couvreur, P., 2006, "Influence of Polysaccharide Coating on the Interactions of Nanoparticles With Biological Systems," *Biomaterials*, **27**(1), pp. 108–118.
- [14] Stutman, D. R., Klein, A., Elaasser, M. S., and Vanderhoff, J. W., 1985, "Mechanism of Core Shell Emulsion Polymerization," *Ind. Eng. Chem. Prod. Res. Dev.*, **24**(3), pp. 404–412.
- [15] Blackburn, W. H., and Lyon, L. A., 2008, "Size-Controlled Synthesis of Monodisperse Core/Shell Nanogels," *Colloid Polym. Sci.*, **286**(5), pp. 563–569.
- [16] Jin, Q., Liu, X., Liu, G., and Ji, J., 2010, "Fabrication of Core or Shell Reversibly Photo Cross-Linked Micelles and Nanogels From Double Responsive Water-Soluble Block Copolymers," *Polymer*, **51**(6), pp. 1311–1319.
- [17] Qi, J. N., Yao, P., He, F., Yu, C. L., and Huang, C. O., 2010, "Nanoparticles With Dextran/Chitosan Shell and BSA/Chitosan Core-Doxorubicin Loading and Delivery," *Int. J. Pharm.*, **393**(1–2), pp. 176–184.
- [18] Deng, W., Li, J., Yao, P., He, F., and Huang, C., 2010, "Green Preparation Process, Characterization and Antitumor Effects of Doxorubicin-BSA-Dextran Nanoparticles," *Macromol. Biosci.*, **10**(10), pp. 1224–1234.

- [19] Lee, H.-S., Stachelek, S. J., Tomczyk, N., Finley, M. J., Composto, R. J., and Eckmann, D. M., 2013, "Correlating Macrophage Morphology and Cytokine Production Resulting From Biomaterial Contact," *J. Biomed. Mater. Res. Part A*, **101A**(1), pp. 203–212.
- [20] Coll Ferrer, M. C., Ferrier, R. C., Jr., Eckmann, D. M., and Composto, R. J., "A Facile Route to Synthesize Nanogels Doped With Silver Nanoparticles," *J. Nanopart. Res.*, (in press).
- [21] Costes, S. V., Daelemans, D., Cho, E. H., Dobbin, Z., Pavlakis, G., and Lockett, S., 2004, "Automatic and Quantitative Measurement of Protein-Protein Colocalization in Live Cells," *Biophys. J.*, **86**(6), pp. 3993–4003.
- [22] Shi, J., Votruba, A. R., Farokhzad, O. C., and Langer, R., 2010, "Nanotechnology in Drug Delivery and Tissue Engineering: From Discovery to Applications," *Nano Lett.*, **10**(9), pp. 3223–3230.
- [23] Oakenfull, D., Pearce, J., and Burley, R., 1997, *Food Proteins and Their Applications*, Vol. 80, Marcel Dekker, New York, pp. 111–142.
- [24] Ibrahim, H. R., Higashiguchi, S., Juneja, L. R., Kim, M., and Yamamoto, T., 1996, "A Structural Phase of Heat-Denatured Lysozyme With Novel Antimicrobial Action," *J. Agric. Food Chem.*, **44**(6), pp. 1416–1423.
- [25] Coll Ferrer, M. C., Yang, S., Eckmann, D. M., and Composto, R. J., 2010, "Creating Biomimetic Polymeric Surfaces by Photochemical Attachment and Patterning of Dextran," *Langmuir*, **26**(17), pp. 14126–14134.
- [26] Ombelli, M., Composto, R. J., Meng, Q. C., and Eckmann, D. M., 2005, "A Quantitative and Selective Chromatography Method for Determining Coverages of Multiple Proteins on Surfaces," *J. Chromatogr., B-Anal. Technol. Biomed. Life Sci.*, **826**(1–2), pp. 198–205.
- [27] Frazier, R. A., Matthijs, G., Davies, M. C., Roberts, C. J., Schacht, E., and Tendler, S. J. B., 2000, "Characterization of Protein-Resistant Dextran Monolayers," *Biomaterials*, **21**(9), pp. 957–966.
- [28] Martwiset, S., Koh, A. E., and Chen, W., 2006, "Nonfouling Characteristics of Dextran-Containing Surfaces," *Langmuir*, **22**(19), pp. 8192–8196.
- [29] Piehler, J., Brecht, A., Hehl, K., and Gauglitz, G., 1999, "Protein Interactions in Covalently Attached Dextran Layers," *Colloids Surf., B*, **13**(6), pp. 325–336.
- [30] Passirani, C., Barratt, G., Devissaguet, J. P., and Labarre, D., 1998, "Interactions of Nanoparticles Bearing Heparin or Dextran Covalently Bound to Poly(Methyl Methacrylate) With the Complement System," *Life Sci.*, **62**(8), pp. 775–785.
- [31] Cansell, M., Parisel, C., Jozefonvicz, J., and Letourneur, D., 1999, "Liposomes Coated With Chemically Modified Dextran Interact With Human Endothelial Cells," *J. Biomed. Mater. Res.*, **44**(2), pp. 140–148.
- [32] Letourneur, D., Parisel, C., Prigent-Richard, S., and Cansell, M., 2000, "Interactions of Functionalized Dextran-Coated Liposomes With Vascular Smooth Muscle Cells," *J. Controlled Release*, **65**(1–2), pp. 83–91.
- [33] Ning, S., Huang, Q., Li, J., Zhang, Y., and Liu, Y.-N., 2011, "Functionalized Dextran-Coated Liposomes for Doxorubicin Loading," *J. Controlled Release*, **152**, pp. E49–E51.
- [34] Du, Y.-Z., Weng, Q., Yuan, H., and Hu, F.-Q., 2011, "Synthesis and Antitumor Activity of Stearate-G-Dextran Micelles for Intracellular Doxorubicin Delivery," *ACS Nano*, **4**(11), pp. 6894–6902.
- [35] Sun, H., Guo, B., Li, X., Cheng, R., Meng, F., Liu, H., and Zhong, Z., 2011, "Shell-Sheddable Micelles Based on Dextran-Ss-Poly(Epsilon-Caprolactone) Diblock Copolymer for Efficient Intracellular Release of Doxorubicin," *Biomacromolecules*, **11**(4), pp. 848–854.
- [36] Choi, K.-C., Bang, J.-Y., Kim, P.-I., Kim, C., and Song, C.-E., 2008, "Amphiphilic B-Incorporated Polymeric Micelles Composed of Poly(D,L-Lactide-Co-Glycolide)/Dextran Graft Copolymer," *Int. J. Pharm.*, **355**(1–2), pp. 224–230.
- [37] Van Thienen, T. G., Raemdonck, K., Demeester, J., and De Smedt, S. C., 2007, "Protein Release From Biodegradable Dextran Nanogels," *Langmuir*, **23**(19), pp. 9794–9801.
- [38] Patnaik, S., Sharma, A. K., Garg, B. S., Gandhi, R. P., and Gupta, K. C., 2007, "Photoregulation of Drug Release in Azo-Dextran Nanogels," *Int. J. Pharm.*, **342**(1–2), pp. 184–193.
- [39] Genz, A. K., Engelhardt, W., and Busche, R., 1999, "Maintenance and Regulation of the pH Microclimate at the Luminal Surface of the Distal Colon of Guinea-Pig," *J. Physiol.*, **517**(2), pp. 507–519.
- [40] Tournier, J. F., Lopez, A., and Tocanne, J. F., 1989, "Effect of Cell Substratum on Lateral Mobility of Lipids in the Plasma-Membrane of Vascular Endothelial Cells," *Exp. Cell Res.*, **181**(1), pp. 105–115.
- [41] Nachman, R. L., and Jaffe, E. A., 2004, "Endothelial Cell Culture: Beginnings of Modern Vascular Biology," *J. Clin. Invest.*, **114**(8), pp. 1037–1040.
- [42] Dobrovolskaia, M. A., Aggarwal, P., Hall, J. B., and McNeil, S. E., 2008, "Preclinical Studies to Understand Nanoparticle Interaction With the Immune System and Its Potential Effects on Nanoparticle Biodistribution," *Mol. Pharm.*, **5**(4), pp. 487–495.
- [43] Tsuchiya, S., Kobayashi, Y., Goto, Y., Okumura, H., Nakae, S., Konno, T., and Tada, K., 1982, "Induction of Maturation in Cultured Human Monocytic Leukemia-Cells by a Phorbol Diester," *Cancer Res.*, **42**(4), pp. 1530–1536.
- [44] Sahay, G., Alakhova, D. Y., and Kabanov, A. V., "Endocytosis of Nanomedicines," *J. Controlled Release*, **145**(3), pp. 182–195.
- [45] Massia, S. P., and Stark, J., 2001, "Immobilized RGD Peptides on Surface-Grafted Dextran Promote Biospecific Cell Attachment," *J. Biomed. Mater. Res.*, **56**(3), pp. 390–399.